

Photonic Molecule Approach to Multiorbital Topology

Maxim Mazanov, Diego Román-Cortés, Gabriel Cáceres-Aravena, Christofer Cid, Maxim A. Gorlach,* and Rodrigo A. Vicencio*



Cite This: *Nano Lett.* 2024, 24, 4595–4601



Read Online

ACCESS |

Metrics & More



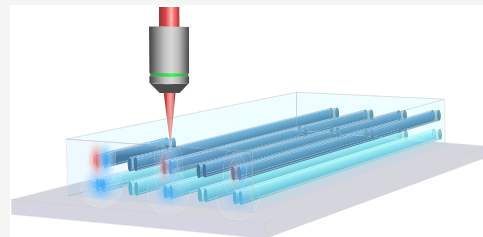
Article Recommendations



Supporting Information

ABSTRACT: The concepts of topology provide a powerful tool to tailor the propagation and localization of the waves. While electrons have only two available spin states, engineered degeneracies of photonic modes provide novel opportunities resembling spin degrees of freedom in condensed matter. Here, we tailor such degeneracies for the array of femtosecond laser written waveguides in the optical range exploiting the idea of photonic molecules: clusters of strongly coupled waveguides. In our experiments, we observe unconventional topological modes protected by the Z_3 invariant arising due to the interplay of interorbital coupling and geometric dimerization mechanism. We track multiple topological transitions in the system with the change in the lattice spacings and excitation wavelength. This strategy opens an avenue for designing novel types of photonic topological phases and states.

KEYWORDS: femtosecond laser writing, photonic orbitals, interorbital coupling, topological photonics, topological edge states



Topological photonics provides a versatile approach to shape the light flows by harnessing the topology of photonic bands.^{1–3} This enables disorder-robust topological states which can be achieved in plasmonic,⁴ photonic,^{5–7} or polaritonic^{8,9} systems operating from radiofrequency^{10,11} to the optical^{5,12} domain.

Experimental realization of optical topological structures is especially demanding because of relatively small feature size, narrow topological bandgaps, and losses. The major strategies to create topological structures for the optical domain include arrays of coupled ring resonators with engineered couplings^{6,13,14} or crystalline topological structures.^{7,12,15–17} While the former approach covers mostly the infrared range being hard to scale toward visible wavelengths, the latter strategy requires carefully designed lattice symmetry and does not provide much flexibility in reconfiguring the topological properties, creating pseudospin degrees of freedom, or tailoring effective spin–orbit interactions. Therefore, these approaches do not unlock the full functionalities available for photonic topological structures.

A recently suggested alternative is to optimize the responses of the *individual meta-atoms* achieving an accidental degeneracy of their modes.^{18–27} Such degenerate modes play a role analogous to the orbital or spin degrees of freedom in condensed matter or cold atom optical lattices.^{28–32} Since the number and the symmetry of the degenerate modes can be tailored on demand, this opens up a rich plethora of novel topological phases. While this appealing strategy can be implemented directly at microwave frequencies,³³ its realization in the visible range is severely hindered due to the fabrication limitations.

Here, we resolve this difficulty by experimentally realizing the concept of *photonic molecules*, a set of closely spaced waveguides which together give rise to photonic orbitals with different symmetries. Employing the femtosecond laser writing technique^{34–36}—an approach that has been consolidated as a key technique in physical lattice studies^{37–40}—to control the refractive index contrast, we create multiorbital photonic lattices such that fundamental *s* (symmetric or bonding) and horizontal excited *p* (antisymmetric or antibonding) modes become degenerate and interact with each other enabling rich physics.

The topological states in such lattice are protected by the Z_3 invariant and arise due to the combination of interorbital coupling and geometric dimerization mechanism. When those mechanisms add up constructively, the array hosts a pair of topological states at each end, which is a unique feature of optical lattices in the absence of long-range interactions. In our experiments, we track the topological transitions upon a change of the wavelength and lattice spacing observing multiple topological states.

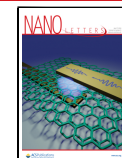
The simplest photonic molecule consists of a couple of closely spaced identical elliptical waveguides [see Figure 1a–top], which give rise to the pair of symmetric (*s*) and antisymmetric (*p*) horizontal modes with the typical intensity

Received: February 9, 2024

Revised: March 27, 2024

Accepted: March 28, 2024

Published: April 4, 2024



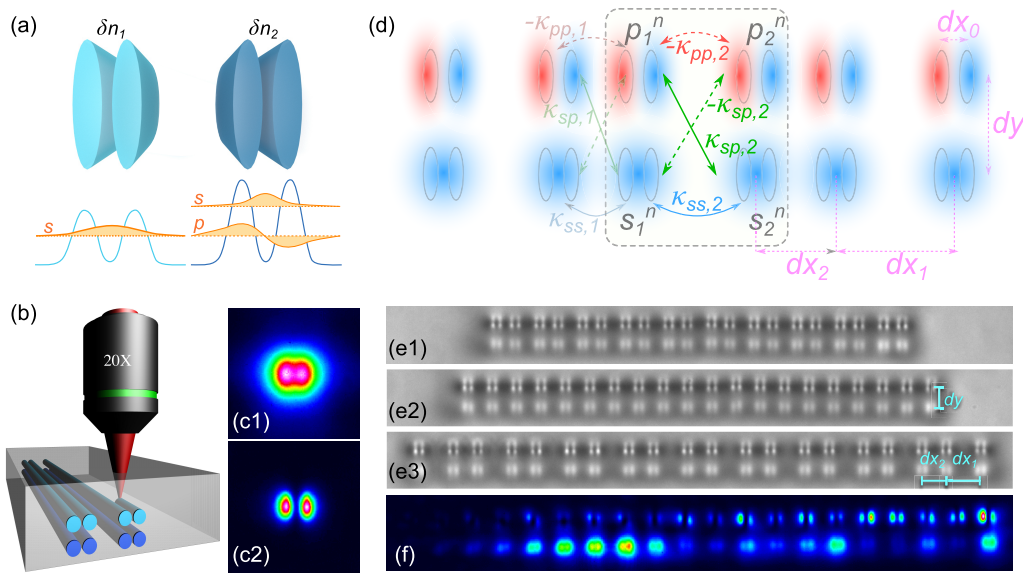


Figure 1. Photonic molecules and the *s*-*p* hybridized topological lattice. (a) Photonic molecules concept. Top: Each molecule is composed of two identical waveguides. We engineer the degeneracy of *s* and *p* modes in two adjacent molecules using different refractive index contrast. (b) Illustration of the femtosecond laser writing technique, where light blue (blue) color represents *s* (*p*) molecules obtained for the different fabrication power. (c1) *s* and (c2) *p* mode intensity profiles obtained after exciting the respective photonic molecule with a 730 nm laser beam. (d) Sketch of the multiorbital topological lattice. Photonic molecules support near-degenerate *s* or *p* modes. Arrows designate the nearest-neighbor couplings, and the dashed box shows the unit cell. (e) White light microscope images of the three fabricated lattices with the lattice spacing dx_1 : (e1) 19 μm , (e2) 25 μm and (e3) 35 μm , for $dx_2 = 25 \mu\text{m}$ and $dy = 20 \mu\text{m}$. (f) Intensity output profile after exciting the *s* molecule at the right edge of the homogeneous lattice shown in (e2).

profiles shown in Figure 1c. While the propagation constants of *s* and *p* modes in a given molecule are strongly different, they can be matched for the adjacent molecules by tuning the refractive index contrast of the waveguides^{20,21} [see Figure 1a-bottom] during the laser writing process illustrated schematically in Figure 1b.

Although the molecular idea is straightforward, its experimental implementation is nontrivial and faces several challenges. First, due to the ellipticity of the waveguide geometry, vertical *p* modes strongly affect the behavior of a single waveguide. However, if a molecule is assembled properly, then *s* and horizontal *p* modes dominate. Another issue is the choice of the distance dx_0 between the waveguides comprising the molecule [see Figure 1d]. From one side, this distance should be larger than the typical width of a single waveguide, which is around 4 μm .³⁵ On the other hand, larger spacings in between the waveguides deteriorate their effective coupling and prevent the formation of clear *s* and *p* molecular modes. After extensive experimental investigations, we optimized the distance $dx_0 = 7 \mu\text{m}$, which yields clear *s* and *p* degenerate modes, as shown in Figure 1c. This trade-off strongly depends on specific fabrication parameters, such as the writing power and the writing velocity as well as the wavelength of excitation (see Supporting Information).

In femtosecond laser-written lattices,³⁵ a standard center-to-center distance of 16 μm is taken as a lower limit for which the tight-binding approach is still valid. Thus, due to the relatively small distance between the waveguides in our molecular setup, the tight-binding model does not describe the formation of molecular *s* and *p* orbitals. However, the interaction of the individual molecules within the molecular lattice is well captured by the coupled-mode approach, which allows us to develop a consistent theoretical description.

As a simple yet nontrivial example of a photonic molecules paradigm, we design and implement a one-dimensional photonic waveguide lattice shown schematically in Figure 1d. Note that the molecules in the upper and lower rows have different refractive index contrast δn , which allows us to match the propagation constant of *s* modes in the lower row to that of the *p* modes in the upper row, thus enabling multiorbital physics. The molecules comprising a single column do not interact with each other since the overlap of their near fields vanishes due to symmetry reasons.

Since the distance between the adjacent molecules in the experimental structure exceeds 19 μm , the physics of the system is captured by the tight-binding model. In the case of equidistant molecular lattice, this requires three coupling parameters: κ_{ss} , κ_{pp} , and $\pm\kappa_{sp}$, describing the interaction of *s* with *s*, *p* with *p*, and *s* with *p* orbitals, respectively. The signs of the coupling constants are defined by the overlap of the respective mode fields.^{19,22}

Even if the lattice consists of equidistant columns, it hosts a pair of topological edge states induced by the interorbital coupling.^{19,22} It is instructive to study the interplay of this mechanism with geometric dimerization of the lattice resembling the celebrated Su–Schrieffer–Heeger model.⁴¹ To that end, we fabricate a set of experimental structures with the dimerization in the lattice spacings (dx_1 , dx_2) between the molecules, Figure 1d,e. As a result, the physics of our system is governed by two competing factors: interference of nearly degenerate *s* and *p* molecular orbitals and geometric dimerization mechanism.

Developing the theoretical description of our system, we adopt the basis of molecular modes $\mathbf{v}^n = (s_1^n, p_1^n, s_2^n, p_2^n)^T$, with the unit cell of the lattice shown in Figure 1d. In these designations, the tight-binding Bloch Hamiltonian reads

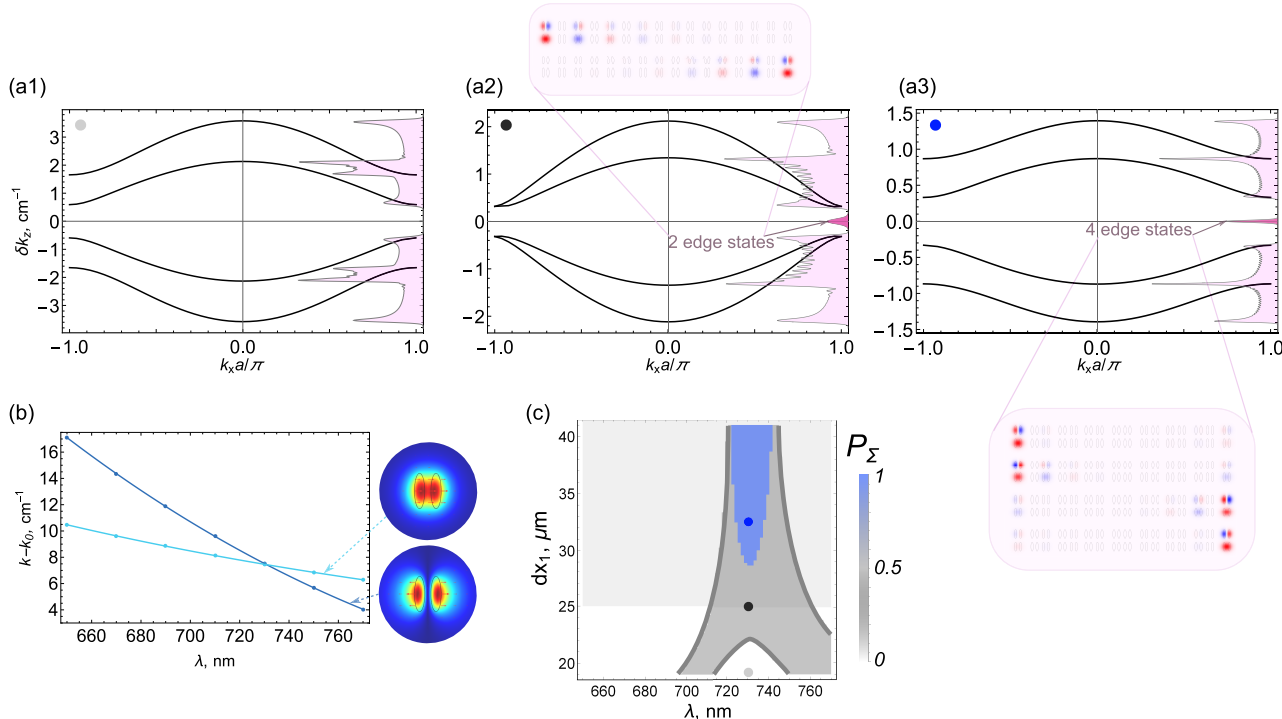


Figure 2. Band topology and edge states for *s-p* hybridized topological lattice. (a) Spectra of propagation constants calculated from eq 1 for $dx_1 = 19 \mu\text{m}$ (a1), $25 \mu\text{m}$ (a2), and $33 \mu\text{m}$ (a3), when $dx_2 = 25 \mu\text{m}$ and $dy = 20 \mu\text{m}$. Insets on the right show the corresponding density of states for the finite 30-cell lattice, with the contribution of hybrid edge states highlighted in dark purple. Graphs near panels a2 and a3 show the calculated edge state profiles in the tight-binding model of an eight-cell lattice. (b) Numerically computed dispersion of the *s* and *p* modes indicating perfect degeneracy at 730 nm calculated for refractive index contrasts $\delta n_1 = 4.132 \times 10^{-4}$, $\delta n_2 = 8.836 \times 10^{-4}$. (c) Topological phase diagram for the Wannier center sum-polarization P_Σ of the central bandgap calculated numerically from the tight-binding model. The region shaded by light gray marks the nontrivial Zak phase of the first (lowest) and third (highest) bandgaps indicating the appearance of practically single-mode edge states.

$$\hat{H}(k_x) = \begin{pmatrix} \hat{\beta} & e^{-ik_x} \hat{k}_{1-} + \hat{k}_{2+} \\ e^{ik_x} \hat{k}_{1+} + \hat{k}_{2-} & \hat{\beta} \end{pmatrix} \quad (1)$$

where k_x is the Bloch wavenumber, $\hat{\beta} = \frac{1}{2}\delta k_{z0} \cdot \hat{\sigma}_z$ and δk_{z0} is the difference in the propagation constants of *s* and *p* orbital modes in an isolated photonic molecule. The coupling matrices read $\hat{k}_{i\pm} = \begin{pmatrix} \kappa_{ss,i} & \pm \kappa_{sp,i} \\ \mp \kappa_{sp,i} & -\kappa_{pp,i} \end{pmatrix}$, with $\kappa_{ss,i}$, $\kappa_{sp,i}$ and $\kappa_{pp,i}$ being the positive interorbital coupling constants that depend on the distances $dx_{1,2}$ and dy between the molecules, as described in Figure 1d. For quantitative predictions, we estimate these coupling coefficients numerically from the splitting of the modes of the two interacting photonic molecules (Supporting Information). The eigenvalue equation then takes the form

$$\hat{H}(\mathbf{k})\mathbf{v} = (k_z - k_0)\mathbf{v} \equiv \delta k_z \mathbf{v} \quad (2)$$

where k_z is the propagation constant of a collective mode in a waveguide array and k_0 is the half-sum of the propagation constants of *s* and *p* modes in an isolated molecule.

While the model above looks simple from the first glance, it features a plethora of topological phases. From an experimental perspective, this physics can be mapped by changing two tuning parameters. One of them is the lattice spacings dx_1 and dx_2 , whose ratio defines the dimerization of the lattice and varies from sample to sample. Another one is the excitation wavelength, which controls the detuning between the

propagation constants of *s* and *p* molecular modes, with a degeneracy condition achieved at $\lambda \approx 730 \text{ nm}$ in the experiments.

By solving the eigenvalue problem eq 2 with the Hamiltonian eq 1, we recover the spectra of the propagation constants in Figure 2a. Interestingly, all calculated spectra are symmetric with respect to the “zero level” corresponding to the propagation constant equal to k_0 . This feature reflects chiral symmetry of the model at perfect mode degeneracy $\delta k_{z0} = 0$ captured by the chiral symmetry operator

$$\hat{\Gamma} = \begin{pmatrix} \hat{I} & 0 \\ 0 & -\hat{I} \end{pmatrix}$$

If the lattice is terminated by a strong coupling link, i.e., the lattice spacing dx_1 at the edge is the smallest, the structure does not support any edge states [Figure 2a1]. In other words, dimerization wins the competition with the mechanism of the mode interference preventing the formation of the edge-localized states.

However, once the lattice is made equidistant, the interference between *s* and *p* modes becomes increasingly important and results in the formation of edge-localized modes [Figure 2a2] in line with the earlier theoretical works.^{19,22} To some approximation, the system is mapped onto the two noninteracting copies of the Su–Schrieffer–Heeger model with the opposite dimerizations yielding a pair of topological edge states at the opposite ends (see Supporting Information). The pairwise degeneracy of the bands at the edges of the Brillouin zone [Figure 2a2] indicates the possibility to choose

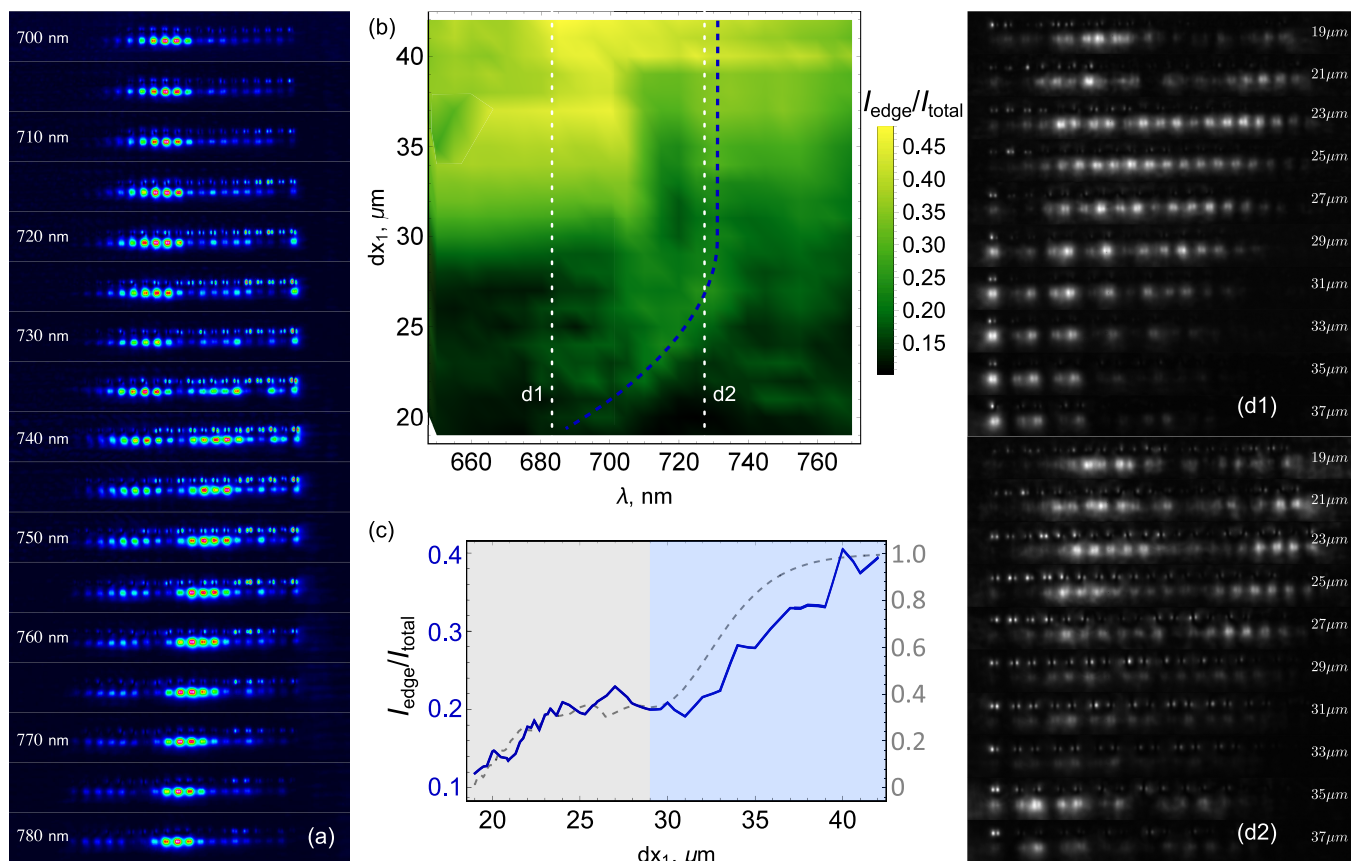


Figure 3. Experimental studies of topological lattices. (a) Intensity output profiles after exciting the homogeneous lattice ($dx_1 = dx_2 = 25 \mu\text{m}$) at the lower right edge s molecule at different wavelengths $\lambda = (700, 780)$ nm. (b) Experimental edge intensity distributions averaged with the first 3 edge columns, for left and right s mode edge excitation versus λ and dx_1 , for fixed $dx_2 = 25$ and $dy = 20 \mu\text{m}$. (c) Comparison of experimental (blue) and rescaled numerical (dotted gray) edge intensity distributions along the dotted blue line shown in (b). A topological transition between the two phases highlighted by gray and blue is observed. (d) Intensity output profiles for the lattice spacings dx_1 indicated at the figure, after exciting the lattice at the left edge s molecule for an excitation wavelength (d1) 680 and (d2) 725 nm, corresponding to the vertical white dashed lines in panel (b).

a smaller unit cell using just two photonic molecules, thus unfolding the Bloch bands.

Finally, terminating the lattice by the weak coupling link ($dx_1 > dx_2$), we ensure that the effects of the lattice dimerization and mode interference add up, which results in the formation of four edge-localized modes existing in a single bandgap [Figure 2a3].

Since bulk polarization in inversion-symmetric systems can take only two values, 0 and $1/2$, it appears insufficient to capture all scenarios of the edge mode formation [Figure 2a1–a3]. This difficulty can be resolved by interpreting ($s + p$) and ($s - p$) mode combinations as effective spin degrees of freedom, retrieving the bulk polarization for each of the pseudospin blocks separately, and adding up the absolute values.

In the general case of nonzero coupling between the introduced pseudospins, the topological Z_3 invariant is formed by the sum of the absolute values of polarization contributions of the two Wannier subsectors being distinct from the total bulk polarization (see the Supporting Information). We thus call it the Wannier center sum-polarization, P_Σ . Note that similarly constructed invariants also appear in two-dimensional higher-order topological structures with pseudospin degree of freedom.^{23,42} Retrieving the Wannier center sum-polarization this way using the numerically obtained couplings and mode

detuning (see Figure 2b), we recover the phase diagram presented in Figure 2c that features three distinct domains.

The standard Su–Schrieffer–Heeger model exhibits only two topological regimes: zero bulk polarization for $dx_1 < dx_2$ ($dx_2 = 25 \mu\text{m}$) and nonzero result for $dx_1 > dx_2$. However, the topological phase diagram of our system, Figure 2c, is richer. If s and p modes are perfectly degenerate, the central bandgap hosts 0, 2, or 4 edge-localized modes, consistent with the calculated Wannier center sum-polarization P_Σ via the bulk-boundary correspondence. This situation persists for moderate detunings between the propagation constants of s and p modes (see the region delimited by the gray thick line). However, once the wavelength is shifted further away from the optimum value of 730 nm, the edge modes in the central bandgap disappear. In this parameter range, the mechanism of mode interference is no longer effective, and hence, the spectra for s and p modes decouple. As a consequence, s and p modes develop their own, practically independent, spectra and topological edge states appear under the usual condition $dx_1 > dx_2$. However, they are no longer hybrid and exist outside of the central bandgap.

To probe our predictions experimentally, we fabricate 25 photonic molecular lattices, having a 70 mm propagation length, with fixed $dy = 20 \mu\text{m}$, $dx_2 = 25 \mu\text{m}$, and dx_1 varying from 18 to 42 μm (see Supporting Information). We excite

those structures via the lower (*s*) photonic molecule either from the left or from the right edge of the array and record the output intensity distribution at different excitation wavelengths by using a supercontinuum laser source.

First, we examine the results for an equidistant molecular lattice [see Figure 3a] in the wavelength range from 700 to 780 nm with the step of 5 nm. Due to the chosen excitation scheme, the output intensity of the *s* sublattice is generally larger than the *p* one. However, those intensities become comparable at wavelengths around 720–750 nm, indicating an efficient interorbital coupling. In the same wavelength range, the output field exhibits localization at the right edge of the array. This points toward the formation of topological edge states possessing a hybrid origin, i.e., having the contribution both from *s* and *p* molecular modes.

To further visualize the emergence of topological edge states in our system, we plot the intensity at the edges of the structure as a function of the excitation wavelength λ and the lattice spacing dx_1 [Figure 3b]. Here, brighter areas correspond to the edge-localized modes, while darker spots show a lack of edge localization arising in the trivial regime and in topological transition points. However, the diagram in Figure 3b does not allow us to differentiate the topological phases with 2 and 4 edge states. To assess this, we chose a specific trajectory on this diagram, shown by a dashed blue line. If the parameters of the system are varied along this trajectory, then analytical calculations suggest that the normalized edge intensity reaches a plateau during the topological transition. Experimental results agree well with this analytical expectation [see Figure 3c] allowing us to approximately capture the topological transition point.

Finally, we examine the role of lattice dimerization for two representative wavelengths. At wavelength $\lambda = 680$ nm, *s* and *p* modes are not degenerate, and hence the formation of the edge modes is defined by the condition $dx_1 > dx_2$. In agreement with this, we observe the formation of an edge-localized field distribution for the lattice spacings dx_1 above 27 μm [Figure 3d1]. In this regime, the *s* mode provides the dominant contribution to the edge intensity. However, the situation changes when the wavelength is shifted toward 725 nm [Figure 3d2] corresponding to the efficient *s-p* coupling (close to zero detuning). The modes of the lattice develop a hybrid structure, while some localization is seen even when the lattice spacing dx_1 is slightly lower than that of dx_2 . Hence, the variations of the two control parameters—wavelength and lattice spacing—enable an exquisite control over topological phases existing in the system.

In summary, the conventional approaches to design topological phases often rely on engineering of the lattice structure. However, manipulating the response of the individual meta-atoms by tailoring the degeneracies of molecular modes with desired symmetry is a promising additional possibility. Here, we bring this strategy to the realm of optical nanostructures, revealing the interplay of interorbital coupling with geometric mechanisms and imaging the topological states experimentally.

As a consequence of those mechanisms, our system allows four topological states to coexist in the same bandgap—a feature previously found only in the lattices with a special pattern of long-range interactions⁴³ and absent in feasible superlattice proposals.^{44–46} In turn, this physics can be further harnessed to coherently control the topological states. Additionally, by manipulating the mode detuning via change

of operating wavelength for a fixed lattice geometry, one can dynamically reconfigure the relevant topological properties.

We anticipate that our approach unlocks an entire plethora of topological phenomena including higher-order topological physics and flat bands at optical wavelengths with possible generalizations toward other platforms such as polaritonics or acoustics. Recently, several works have been proposed to harness multiorbital physics to tailor the topological properties of two-dimensional photonic systems such as the higher-order crystalline topology in naturally p_x-p_y -hybridized kagome lattices,^{47,48} higher-order quadrupole topology in a bipartite square *s-p*-hybridized lattice,⁴⁹ and other unconventional types of multipole topology,³³ as well as spinful generalizations of known higher-order topological insulators.^{23,42,50}

We believe that our approach of utilizing photonic molecules to tune the relevant orbital degeneracies could allow scaling more of these proposals toward the optical range where such degeneracy fine-tuning may otherwise be challenging.

ASSOCIATED CONTENT

Supporting Information

The Supporting Information is available free of charge at <https://pubs.acs.org/doi/10.1021/acs.nanolett.4c00728>.

Discussion of the chiral symmetry of the model for the perfectly degenerate modes; decomposition of the tight-binding effective Hamiltonian into two pseudospin blocks with nontrivial Zak phases; topological winding number calculation; Wannier center sum-polarization topological invariant calculation; evolution of the finite-lattice spectrum with and without disorder; numerical characterization of the coupling constants between orbital modes of photonic molecules; details of experimental fabrication, calibration, and optimization of the femtosecond photonic lattices; figures supporting the Supporting Information (PDF)

AUTHOR INFORMATION

Corresponding Authors

Maxim A. Gorlach — School of Physics and Engineering, ITMO University, Saint Petersburg 197101, Russia;
ORCID: [0000-0002-7880-8953](https://orcid.org/0000-0002-7880-8953); Email: m.gorlach@metalab.ifmo.ru

Rodrigo A. Vicencio — Departamento de Física and Millenium Institute for Research in Optics—MIRO, Facultad de Ciencias Físicas y Matemáticas, Universidad de Chile, 8370448 Santiago, Chile; Email: rvcencio@uchile.cl

Authors

Maxim Mazanov — School of Physics and Engineering, ITMO University, Saint Petersburg 197101, Russia

Diego Román-Cortés — Departamento de Física and Millenium Institute for Research in Optics—MIRO, Facultad de Ciencias Físicas y Matemáticas, Universidad de Chile, 8370448 Santiago, Chile; ORCID: [0000-0001-8844-4236](https://orcid.org/0000-0001-8844-4236)

Gabriel Cáceres-Aravena — Departamento de Física and Millenium Institute for Research in Optics—MIRO, Facultad de Ciencias Físicas y Matemáticas, Universidad de Chile, 8370448 Santiago, Chile; Institute of Physics, University of Rostock, 18051 Rostock, Germany

Christofer Cid — Departamento de Física and Millenium Institute for Research in Optics—MIRO, Facultad de Ciencias

Físicas y Matemáticas, Universidad de Chile, 8370448 Santiago, Chile

Complete contact information is available at:
<https://pubs.acs.org/10.1021/acs.nanolett.4c00728>

Notes

The authors declare no competing financial interest.

ACKNOWLEDGMENTS

Tight-binding calculations were supported by Priority 2030 Federal Academic Leadership Program. Evaluation of Z_3 topological invariant was supported by the Russian Science Foundation (grant No. 23-72-10026). Experimental studies were supported by Millennium Science Initiative Program ICN17012 and FONDECYT Grants 1191205 and 1231313. M.M. and M.A.G. acknowledge partial support from the Foundation for the Advancement of Theoretical Physics and Mathematics “Basis”. G.C.-A. acknowledges the Deutsche Forschungsgemeinschaft (DFG, German Research Foundation) through IRTG 2676/1 ‘Imaging of Quantum Systems’, project no. 437567992.

REFERENCES

- (1) Lu, L.; Joannopoulos, J. D.; Soljačić, M. Topological photonics. *Nat. Photonics* **2014**, *8*, 821–829.
- (2) Lu, L.; Joannopoulos, J. D.; Soljačić, M. Topological states in photonic systems. *Nat. Phys.* **2016**, *12*, 626–629.
- (3) Ozawa, T.; Price, H. M.; Amo, A.; Goldman, N.; Hafezi, M.; Lu, L.; Rechtsman, M. C.; Schuster, D.; Simon, J.; Zilberberg, O.; Carusotto, I. Topological photonics. *Rev. Mod. Phys.* **2019**, *91*, No. 015006.
- (4) Cheng, Q.; Pan, Y.; Wang, Q.; Li, T.; Zhu, S. Topologically protected interface mode in plasmonic waveguide arrays. *Laser & Photonics Reviews* **2015**, *9*, 392–398.
- (5) Rechtsman, M. C.; Zeuner, J. M.; Plotnik, Y.; Lumer, Y.; Podolsky, D.; Dreisow, F.; Nolte, S.; Segev, M.; Szameit, A. Photonic Floquet topological insulators. *Nature* **2013**, *496*, 196–200.
- (6) Hafezi, M.; Mittal, S.; Fan, J.; Migdall, A.; Taylor, J. M. Imaging topological edge states in silicon photonics. *Nat. Photonics* **2013**, *7*, 1001–1005.
- (7) Barik, S.; Karasahin, A.; Flower, C.; Cai, T.; Miyake, H.; DeGottardi, W.; Hafezi, M.; Waks, E. A topological quantum optics interface. *Science* **2018**, *359*, 666–668.
- (8) Karzig, T.; Bardyn, C.-E.; Lindner, N. H.; Refael, G. Topological Polaritons. *Physical Review X* **2015**, *5*, No. 031001.
- (9) Klempt, S.; Harder, T. H.; Egorov, O. A.; Winkler, K.; Ge, R.; Bandres, M. A.; Emmerling, M.; Worschech, L.; Liew, T. C. H.; Segev, M.; Schneider, C.; Höfling, S. Exciton-polariton topological insulator. *Nature* **2018**, *562*, 552–556.
- (10) Yves, S.; Fleury, R.; Berthelot, T.; Fink, M.; Lemoult, F.; Lerosey, G. Crystalline metamaterials for topological properties at subwavelength scales. *Nat. Commun.* **2017**, *8*, 16023.
- (11) Yang, Y.; Gao, Z.; Xue, H.; Zhang, L.; He, M.; Yang, Z.; Singh, R.; Chong, Y.; Zhang, B.; Chen, H. Realization of a three-dimensional photonic topological insulator. *Nature* **2019**, *565*, 622–626.
- (12) Noh, J.; Benalcazar, W. A.; Huang, S.; Collins, M. J.; Chen, K. P.; Hughes, T. L.; Rechtsman, M. C. Topological protection of photonic mid-gap defect modes. *Nat. Photonics* **2018**, *12*, 408–415.
- (13) Hafezi, M.; Demler, E. A.; Lukin, M. D.; Taylor, J. M. Robust optical delay lines with topological protection. *Nat. Phys.* **2011**, *7*, 907–912.
- (14) Mittal, S.; Orre, V. V.; Zhu, G.; Gorlach, M. A.; Poddubny, A.; Hafezi, M. Photonic quadrupole topological phases. *Nat. Photonics* **2019**, *13*, 692.
- (15) Wu, L.-H.; Hu, X. Scheme for Achieving a Topological Photonic Crystal by Using Dielectric Material. *Phys. Rev. Lett.* **2015**, *114*, 223901.
- (16) Gorlach, M. A.; Ni, X.; Smirnova, D. A.; Korobkin, D.; Zhirihihin, D.; Slobozhanyuk, A. P.; Belov, P. A.; Alù, A.; Khanikaev, A. B. Far-field probing of leaky topological states in all-dielectric metasurfaces. *Nat. Commun.* **2018**, *9*, 909.
- (17) Parappurath, N.; Alpegiani, F.; Kuipers, L.; Verhagen, E. Direct observation of topological edge states in silicon photonic crystals: Spin, dispersion, and chiral routing. *Science. Advances* **2020**, *6*, No. eaaw4137.
- (18) Cáceres-Aravena, G.; Vicencio, R. A. Perfect localization on flat-band binary one-dimensional photonic lattices. *Phys. Rev. A* **2019**, *100*, No. 013803.
- (19) Cáceres-Aravena, G.; Torres, L. E. F. F.; Vicencio, R. A. Topological and flat-band states induced by hybridized linear interactions in one-dimensional photonic lattices. *Phys. Rev. A* **2020**, *102*, No. 023505.
- (20) Guzmán-Silva, D.; Cáceres-Aravena, G.; Vicencio, R. A. Experimental Observation of Interorbital Coupling. *Phys. Rev. Lett.* **2021**, *127*, No. 066601.
- (21) Cáceres-Aravena, G.; Guzmán-Silva, D.; Salinas, I.; Vicencio, R. A. Controlled Transport Based on Multiorbital Aharonov-Bohm Photonic Caging. *Phys. Rev. Lett.* **2022**, *128*, 256602.
- (22) Savelev, R. S.; Gorlach, M. A. Topological states in arrays of optical waveguides engineered via mode interference. *Phys. Rev. B* **2020**, *102*, 161112.
- (23) Mazanov, M.; Gorlach, M. A. Tailoring higher-order topological phases via orbital hybridization. *Phys. Rev. B* **2022**, *105*, 205117.
- (24) Mikhin, A. O.; Rutckaia, V.; Savelev, R. S.; Sinev, I. S.; Alù, A.; Gorlach, M. A. Coherent Control of Topological States in an Integrated Waveguide Lattice. *Nano Lett.* **2023**, *23*, 2094–2099.
- (25) Huang, X.; Lai, Y.; Hang, Z. H.; Zheng, H.; Chan, C. T. Dirac cones induced by accidental degeneracy in photonic crystals and zero-refractive-index materials. *Nat. Mater.* **2011**, *10*, 582.
- (26) Sakoda, K. Proof of the universality of mode symmetries in creating photonic Dirac cones. *Opt. Express* **2012**, *20*, 25181–25194.
- (27) Gorbach, A. V.; Beer, J.; Souslov, A. Topological edge states in equidistant arrays of lithium niobate nano-waveguides. *Opt. Lett.* **2023**, *48*, 1982–1985.
- (28) Li, X.; Liu, W. V. Physics of higher orbital bands in optical lattices: a review. *Rep. Prog. Phys.* **2016**, *79*, 116401.
- (29) Li, X.; Zhao, E.; Vincent Liu, W. Topological states in a ladder-like optical lattice containing ultracold atoms in higher orbital bands. *Nat. Commun.* **2013**, *4*, 1523.
- (30) Pelegri, G.; Marques, A. M.; Dias, R. G.; Daley, A. J.; Mompart, J.; Ahufinger, V. Topological edge states and Aharonov-Bohm caging with ultracold atoms carrying orbital angular momentum. *Phys. Rev. A* **2019**, *99*, No. 023613.
- (31) Yin, S.; Baarsma, J. E.; Heikkinen, M. O. J.; Martikainen, J.-P.; Törmä, P. Superfluid phases of fermions with hybridized sand porbitals. *Phys. Rev. A* **2015**, *92*, No. 053616.
- (32) Wu, C.; Bergman, D.; Balents, L.; Das Sarma, S. Flat bands and Wigner crystallization in the honeycomb optical lattice. *Phys. Rev. Lett.* **2007**, *99*, No. 070401.
- (33) Mazanov, M.; Kupriianov, A. S.; Savelev, R. S.; He, Z.; Gorlach, M. A. Multipole higher-order topology in a multimode lattice. *arXiv:2207.11348* **2022**, DOI: [10.48550/arXiv.2207.11348](https://doi.org/10.48550/arXiv.2207.11348).
- (34) Davis, K. M.; Miura, K.; Sugimoto, N.; Hirao, K. Writing waveguides in glass with a femtosecond laser. *Opt. Lett.* **1996**, *21*, 1729–1731.
- (35) Szameit, A.; Blömer, D.; Burghoff, J.; Schreiber, T.; Pertsch, T.; Nolte, S.; Tünnermann, A.; Lederer, F. Discrete nonlinear localization in femtosecond laser written waveguides in fused silica. *Opt. Express* **2005**, *13*, 10552–10557.
- (36) Flaminii, F.; Magrini, L.; Rab, A. S.; Spagnolo, N.; DAmbrosio, V.; Mataloni, P.; Sciarrino, F.; Zandrini, T.; Crespi, A.; Ramponi, R.; Osellame, R. Thermally reconfigurable quantum photonic circuits at

- telecom wavelength by femtosecond laser micromachining. *Light: Science & Applications* **2015**, *4*, e354–e354.
- (37) Rechtsman, M. C.; Zeuner, J. M.; Plotnik, Y.; Lumer, Y.; Podolsky, D.; Dreisow, F.; Nolte, S.; Segev, M.; Szameit, A. Photonic Floquet topological insulators. *Nature* **2013**, *496*, 196–200.
- (38) Vicencio, R. A.; Cantillano, C.; Morales-Inostroza, L.; Real, B.; Mejía-Cortés, C.; Weimann, S.; Szameit, A.; Molina, M. I. Observation of Localized States in Lieb Photonic Lattices. *Phys. Rev. Lett.* **2015**, *114*, 245503.
- (39) Mukherjee, S.; Spracklen, A.; Choudhury, D.; Goldman, N.; Öhberg, P.; Andersson, E.; Thomson, R. R. Observation of a Localized Flat-Band State in a Photonic Lieb Lattice. *Phys. Rev. Lett.* **2015**, *114*, 245504.
- (40) El Hassan, A.; Kunst, F. K.; Moritz, A.; Andler, G.; Bergholtz, E. J.; Bourennane, M. Corner states of light in photonic waveguides. *Nat. Photonics* **2019**, *13*, 697–700.
- (41) Su, W. P.; Schrieffer, J. R.; Heeger, A. J. Solitons in Polyacetylene. *Phys. Rev. Lett.* **1979**, *42*, 1698–1701.
- (42) Gladstein Gladstone, R.; Jung, M.; Shvets, G. Spin-Polarized Fractional Corner Charges and Their Photonic Realization. *Phys. Rev. Lett.* **2022**, *128*, No. 026801.
- (43) Maffei, M.; Dauphin, A.; Cardano, F.; Lewenstein, M.; Massignan, P. Topological characterization of chiral models through their long time dynamics. *New J. Phys.* **2018**, *20*, No. 013023.
- (44) Longhi, S. Probing topological phases in waveguide superlattices. *Opt. Lett.* **2019**, *44*, 2530–2533.
- (45) Midya, B.; Feng, L. Topological multiband photonic superlattices. *Phys. Rev. A* **2018**, *98*, No. 043838.
- (46) Wei, R.; Zhang, Q.; Yang, D.; Huang, X.; Pan, Q.; Kang, J.; Qiu, J.; Yang, Z.; Dong, G. Realization of one-dimensional $2n$ -root topological states in photonic lattices. *Sci. China Technol. Sci.* **2024**, *67*, 98–104.
- (47) Zhang, Y.; Bongiovanni, D.; Wang, Z.; Wang, X.; Xia, S.; Hu, Z.; Song, D.; Jukić, D.; Xu, J.; Morandotti, R.; Buljan, H.; Chen, Z. Realization of photonic p-orbital higher-order topological insulators. *eLight* **2023**, *3*, 5.
- (48) Lu, X.; Chen, Y.; Chen, H. Orbital corner states on breathing kagome lattices. *Phys. Rev. B* **2020**, *101*, 195143.
- (49) Schulz, J.; Noh, J.; Benalcazar, W. A.; Bahl, G.; von Freymann, G. Photonic quadrupole topological insulator using orbital-induced synthetic flux. *Nat. Commun.* **2022**, *13*, 6597.
- (50) Chen, Y.; Meng, F.; Lan, Z.; Jia, B.; Huang, X. Dual-Polarization Second-Order Photonic Topological Insulators. *Phys. Rev. Appl.* **2021**, *15*, No. 034053.